NANO LETTERS

Letter

pubs.acs.org/NanoLett

Dynamic Charge Carrier Trapping in Quantum Dot Field Effect Transistors

Yingjie Zhang,[†,‡] Qian Chen,[§,∥] A. Paul Alivisatos,[‡,§,⊥,#] and Miquel Salmeron*[,‡,⊥]

[†]Applied Science and Technology Graduate Program, University of California at Berkeley, Berkeley, California 94720, United States
[‡]Materials Sciences Division, Lawrence Berkeley National Laboratory, Berkeley, California 94720, United States
[§]Department of Chemistry, University of California at Berkeley, Berkeley, California 94720, United States
[∥]Miller Institute for Basic Research in Science, University of California at Berkeley, Berkeley, California 94720, United States
[⊥]Department of Materials Science and Engineering, University of California at Berkeley, Berkeley, California 94720, United States
[#]Kavli Energy NanoScience Institute, Berkeley, California 94720, United States

Supporting Information

ABSTRACT: Noncrystalline semiconductor materials often exhibit hysteresis in charge transport measurements whose mechanism is largely unknown. Here we study the dynamics of charge injection and transport in PbS quantum dot (QD) monolayers in a field effect transistor (FET). Using Kelvin probe force microscopy, we measured the temporal response of the QDs as the channel material in a FET following step function changes of gate bias. The measurements reveal an exponential decay of mobile carrier density with time constants of 3−5 s for holes and ∼10 s for electrons. An Ohmic behavior, with uniform carrier density, was observed along the channel during the injection and transport processes. These slow, uniform carrier trapping processes are reversible, with time constants that depend critically on the gas environment. We propose that the underlying mechanism is some reversible electrochemical process involving dissociation and diffusion of water and/or oxygen related species. These trapping processes are dynamically activated by the injected charges, in contrast with static electronic traps whose presence is independent of the charge state. Understanding and controlling these processes is important for improving the performance of electronic, optoelectronic, and memory devices based on disordered semiconductors.

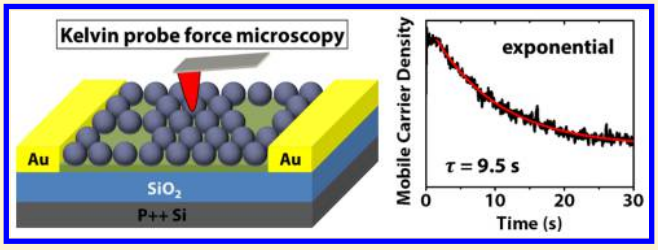

KEYWORDS: *Colloidal quantum dot, dynamic charge trapping, charge transport, field effect transistor, hysteresis, bias stress*

Colloidal quantum dots (QDs), with tunable band gap and electronic structure, are being explored for various electronic and optoelectronic device applications, such as field effect transistors (FETs), photodetectors, and solar cells.[1−4] The past decade has seen tremendous progress in the optimization of QD based devices, focusing on controlling surface capping ligands for better surface passivation and enhanced carrier mobility and lifetime.[5] Despite all these efforts, an intriguing phenomenon that still remains poorly understood is charge carrier trapping, which is observed in all kinds of QD systems.[6−10] For individual QDs, the long-standing mystery of fluorescence blinking phenomena is thought to be related to charge trapping in defect states, although the nature of the defects and trapping mechanism is not understood.[8−10] For QD devices, deep traps assist carrier recombination (Shockley−Read−Hall recombination), limiting the optoelectronic device efficiency. Shallow traps, however, can be utilized to enhance carrier lifetime for improving the gain in photoconductors.[2,11] In FETs that operate under dark conditions, although it has been recently observed that certain deep defect states can actually assist carrier transport,[7,12] QD films still suffer from significant hysteresis effects where the source-drain current decays substantially in the scale of seconds after charge injection.[13] These effects were found to be independent of the gate dielectric and were thus attributed to the intrinsic properties of PbS QDs. However, no quantitative information on carrier density was presented, and the carrier trapping mechanism is still unresolved. Traditional methods of carrier dynamics analysis (e.g., photoluminescence, transient absorption and transient photocurrent, current−voltage, and capacitance voltage measurements) provide insights into the trapping behavior but have so far failed to uncover the underlying microscopic mechanisms.[9,14]

In this work, we employ Kelvin probe force microscopy (KPFM) to analyze the hysteresis behavior of charge injection and transport in monolayers of PbS QDs. Previous work on the hysteresis in QD FETs only measured source-drain current, which is a convolution of charge injection and transport,[13] and possibly contact resistance. Moreover, the transport current has contribution from both mobility and carrier density. Here we

Received: April 13, 2015
Revised: June 6, 2015
Published: June 23, 2015

DOI: 10.1021/acs.nanolett.5b01429
Nano Lett. 2015, 15, 4657−4663

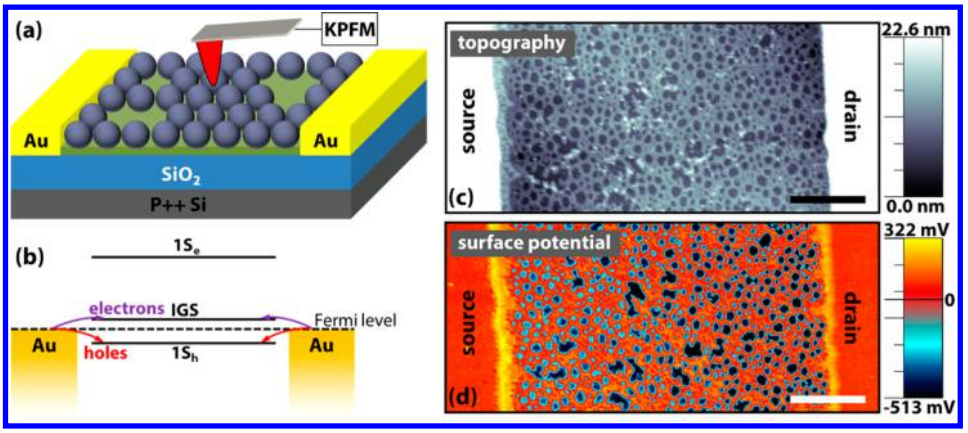

Figure 1. Schematic setup of the Kelvin probe force microscopy (KPFM) and FET measurement. (a) Schematic PbS QD submonolayer FET probed by KPFM. Channel length is ~20 μm, and width is 1 mm. Oxide thickness is 300 nm. The green line represents an OTS monolayer on top of the SiO_2 substrate. (b) Energy level alignment diagram of the FET. The Fermi level in the QDs is located between the in-gap states (IGS) and the valence band ($1S_h$) states. The IGS are responsible for electron transport in the dark. (c,d) Topographic and surface potential maps of the FET. Scale bar: 4 μm. The brighter parts inside the channel region (c) are due to the QD monolayer, corresponding to the higher surface potential regions (d). The darker spots (with lower surface potential) in the channel correspond to the OTS passivated oxide surface not covered by QDs.

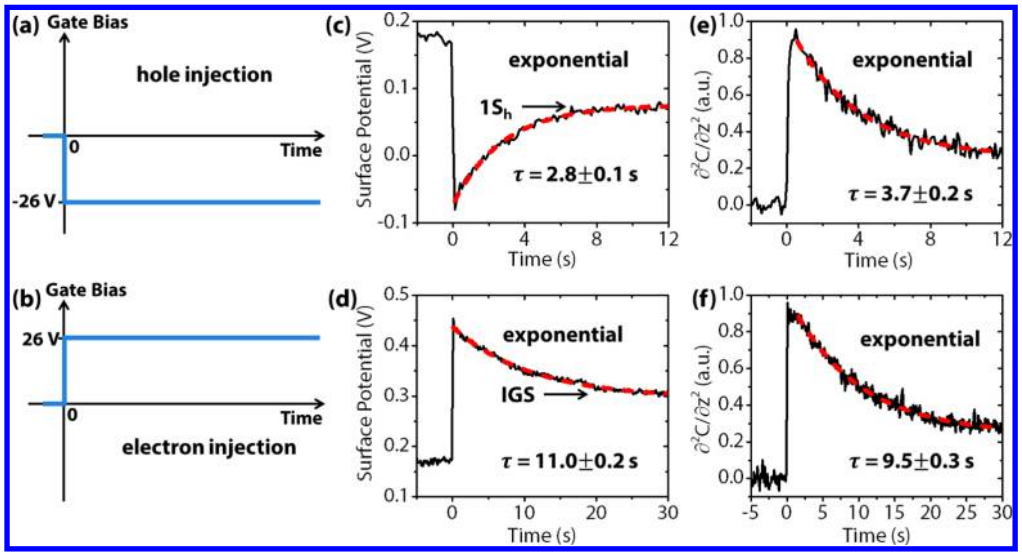

Figure 2. Charge injection dynamics of PbS QD FETs. (a,b) The ∓26 V gate bias step function applied at time zero to inject holes and electrons, respectively. (c–f) Transient dynamics of surface potential and capacitance ($\partial^2C/\partial z^2$), as labeled. Upper panels correspond to hole injection, lower panels to electron injection. Black solid curves are raw data, while red dashed curves are fittings. The fitting parameters together with the standard errors are shown in each figure. The long-time equilibrium surface potential values correspond to the $1S_h$ states and IGS, for holes and electrons, respectively, as marked in (c) and (d).

directly measure the transient behavior of carrier density, which we believe can clarify the mechanism of charge trapping.

Experimental Setup. The schematic of the FET and KPFM setup used in our measurements is shown in Figure 1a. PbS QDs with 5.5 nm diameter and 0.9 eV bandgap were deposited on the FET substrates passivated with octadecyltrichlorosilane (OTS) to remove oxide surface charge traps. The QDs were treated with 1,2-ethanedithiol (EDT), which replaces the native oleate ligands on the surface, reduces the interparticle distance, and activates charge transport.[12,15,16] Previous work by Nagpal et al. indicates that in-gap states (IGS) can assist carrier transport in the EDT treated PbS QD films.[7] Our previous results showed that under dark conditions hole transport occurs via valence band ($1S_h$) states, while electron transport takes place via IGS (Figure 1b), ~0.2 eV above the $1S_h$ states.[12]

A home-built single pass, frequency modulation KPFM was implemented based on an atomic force microscope (AFM) and used for surface potential measurements with a resolution around 10 mV.[12,17] All the measurements were done in an inert nitrogen atmosphere (with a relative humidity of <0.5%, the detection limit of our hygrometer), except when specially noted. During KPFM measurements, a $V_{DC} + V_{AC}\cos(\omega t)$ bias is applied to the metal-coated AFM tip, with $V_{AC} = 2$ V = 2 kHz. With the sample grounded, the AC tip bias yields components of the cantilever phase shift at ω and 2ω, respectively:

$$\Delta f_{\omega} \propto \frac{\partial^2 C}{\partial z^2}(CPD - V_{DC})V_{AC} \quad (1)$$

$$\Delta f_{2\omega} \propto \frac{\partial^2 C}{\partial z^2}{V_{AC}}^2 \quad (2)$$

DOI: 10.1021/acs.nanolett.5b01429
Nano Lett. 2015, 15, 4657–4663

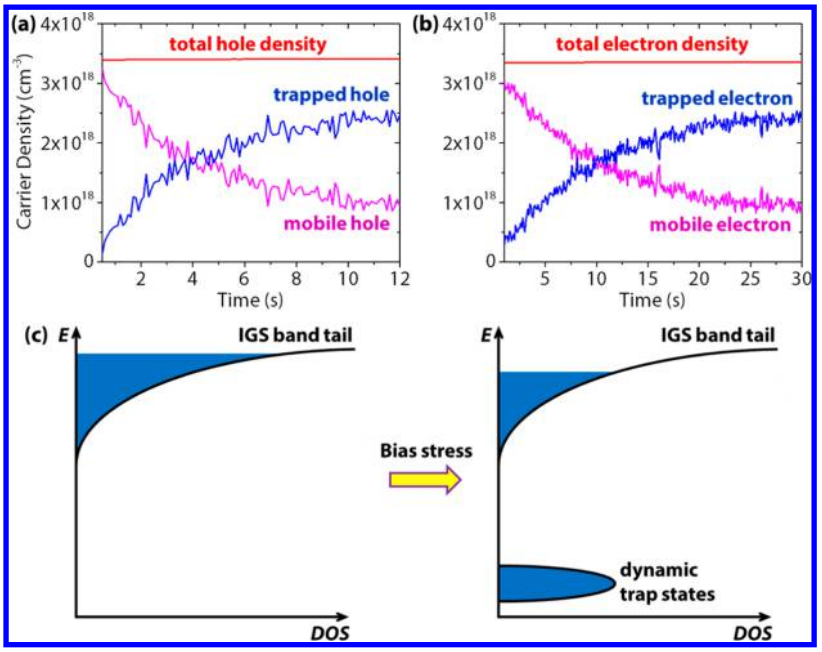

Figure 3. Dynamic carrier trapping mechanism. (a,b) Carrier density decay of holes and electrons, respectively, after the ∓26 V gate bias, including the total density, mobile, and trapped carrier density. (c) The left schematic shows the injected electrons filling part of the IGS band (blue region) right after charge injection. The right schematic shows the trap states created after charge injection, which capture electrons from the IGS and gradually become filled. These dynamic traps, which do not exist before charge injection, can have an energy level lower than the $1S_h$ states.

where CPD is the tip−sample contact potential difference, C is the capacitance between AFM tip and the sample, and z is the tip−sample distance. V_{DC} is adjusted to maintain $\Delta f_\omega = 0$, and at the same time V_{DC} is recorded as the CPD. The surface potential (V_{sf}) signal of the sample is obtained from CPD calibrated by setting the CPD of the nearby grounded Au electrode (here the deposited QDs were scratched away) to zero. Since the work function of Au (5.1 eV) is the same as that of the gate (p++ Si substrate), the calibrated value of V_{sf} corresponds to the actual potential difference between the channel and the gate in the FET. $\Delta f_{2\omega}$ is also recorded as the $\partial^2C/\partial z^2$ signal, providing information on the tip−sample capacitance. The spatial resolution of the V_{sf} and $\partial^2C/\partial z^2$ signal is 20−50 nm.

The charge injected into the PbS film following a step change in gate bias can be followed by measuring V_{sf} as a function of time. The charge density can be obtained using the capacitor relation

$$N = \frac{C_{ox}}{t_c e}|V_g - V_{sf}| \tag{3}$$

where C_{ox} is the capacitance per unit area of the SiO_2, t_c is the channel thickness (~5.5 nm), and e is the absolute value of the elementary charge. Meanwhile, the capacitance signal ($\partial^2C/\partial z^2$) is a measure of mobile carrier density N_m (density of free moving carriers in response to the tip's AC bias with $\omega = 2kHz$).[18]

The simultaneously recorded topography and surface potential images of a FET channel area is shown in Figure 1c,d. The images show that the QD film has submonolayer coverage, with a porous structure connecting the source and drain electrodes. At a gate bias $V_g = 0$, the V_{sf} of the QDs in the channel region is 150−200 mV, 500−600 mV higher than that of the OTS passivated oxide surface (Supporting Information).

Charge Trapping Dynamics upon Injection. With the tip placed 5−10 nm above the QD monolayer in the channel region, we probed the transient charge injection and relaxation process by simultaneously recording the source current (current flowing out of the source electrode), surface potential, and $\partial^2C/\partial z^2$ following a step change in the gate bias (Figure 2). Previously we found that at steady state V_{sf} is pinned at $1S_h$ states and at IGS when $V_g < \sim -15$ V and when $V_g > \sim 15$ V.[12] We thus applied a gate bias step from 0 to ±26 V to inject carriers into conductive states (Figure 2a,b), with source and drain grounded. Figure 2c−f shows the temporal response of V_{sf} and $\partial^2C/\partial z^2$ following the bias step. Since no source-drain bias was applied, there is no steady-state current, although we did observe transient current due to slow charge injection into the channel (Supporting Information). The surface potential transients can be fitted with single exponential decays, with τ = 2.8 and 11.0 s for holes and electrons, respectively. The $\partial^2C/\partial z^2$ transients also follow exponential decays, with τ = 3.7 and 9.5 s for holes and electrons, respectively. In both transients the electron relaxation time is longer than that of hole relaxation. A different gate bias of ±39 V was applied and the time constants were found to be similar.

The V_{sf} and $\partial^2C/\partial z^2$ transients, measured inside the channel, were found to be independent of the distance to the source/drain electrodes, revealing that the observed transients are not due to charge diffusion inside the QDs. Upon hole injection, V_{sf} increases from −0.08 to 0.08 V, corresponding to a slight increase of charge density from 3.39×10^{18} cm^{-3} to 3.41×10^{18} cm^{-3} (calculated using eq 3), as shown in Figure 3a. For electrons, V_{sf} decreases from 0.44 to 0.30 V, corresponding to a minute increase of charge density from 3.34×10^{18} cm^{-3} to 3.36×10^{18} cm^{-3} (eq 3, Figure 3b). In contrast, the $\partial^2C/\partial z^2$ signal, a measure of mobile carrier density, decreased significantly (Figure 2e,f). The capacitance curves are linearly normalized such that $\partial^2C/\partial z^2$ is 0 at $t < 0$ and 1 at $t = 0$ (determined by the exponential fit). Assuming that the injected charge carriers are all mobile at $t = 0$ (with an initial density of N_0), the mobile carrier density can be written as

DOI: 10.1021/acs.nanolett.5b01429
Nano Lett. 2015, 15, 4657−4663

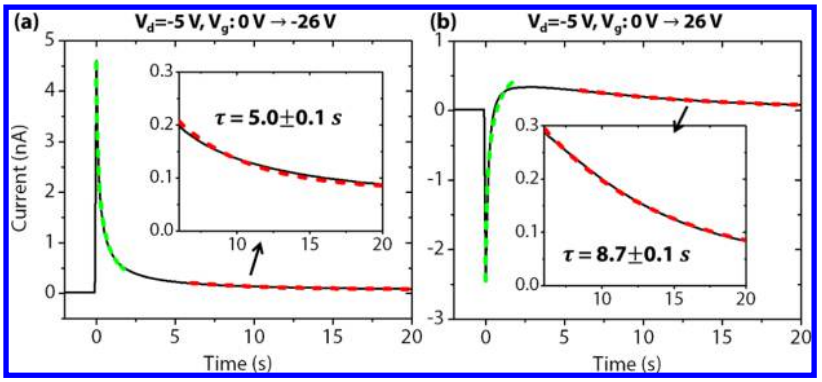

Figure 4. Current injection and transport dynamics at a drain bias of $V_d = -5$ V, after the application of a gate bias step from zero to ∓26 V, as labeled: (a,b) hole and electron dynamics. Insets are expansions of the curves in the 6−20 s time window.

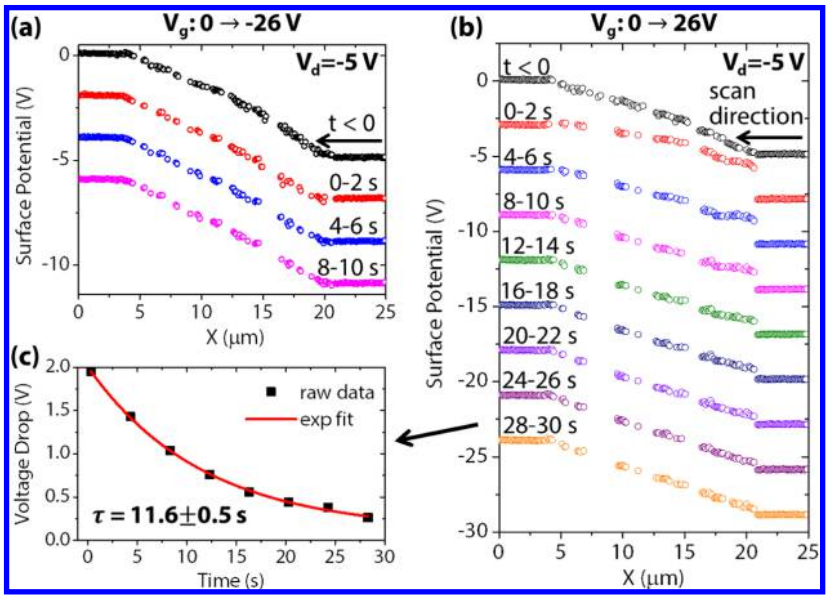

Figure 5. Dynamics of the surface potential profile across the channel at $V_d = -5$ V, after the application of a gate bias step of ∓26 V: (a,b) hole and electron dynamics, and each curve corresponds to the surface potential profile covering the source (left), channel (middle), and drain (right). The tip was scanned from the right to the left within the labeled time range (2 s per line). The black curves correspond to the surface potential profiles at zero gate bias. Linear offsets were applied in subsequent curves for clarity. Only the surface potential data on the QD monolayer regions are shown (data from the uncovered regions exposing the oxide were removed), resulting in gaps in the data lines. (c) Voltage drop vs time at the drain contact shown in (b). Red line is the exponential fit.

$$N_m = N_0 \partial^2 C / \partial z^2 \quad (4)$$

when $t > 0$. The trapped carrier density can thus be obtained as

$$N_t = N - N_m \quad (5)$$

The mobile and trapped density of holes and electrons determined from eqs 4 and 5 are shown in Figure 3a,b. We can see that the initially injected free carriers gradually become immobile, in the time scale of 3.7 s for holes and 9.5 s for electrons. The density of mobile carriers decreases significantly during the transient trapping process, to ∼30% of the initial value in 12 s for holes and in 30 s for electrons.

Due to insufficient screening of the gate field during charge injection,[17] the actual Fermi level change can only be smaller than the change of eV_{sf} (∼0.15 eV). Since the final V_{sf} level matches well with the IGS for electron injection and with valence band states for hole injection, we can conclude that the charges were initially injected into the IGS/$1S_h$ states and were gradually trapped, with a slight change of Fermi level. The proposed mechanism of the carrier relaxation transients is shown in Figure 3c. Since the decay of carrier density is a single exponential, we expect that a single trapping process is dominant. Hole injection follows the same trend as in the case of electrons, i.e., the holes gradually falling into traps above the valence band edge.

Charge Transport Dynamics upon Injection. Having observed the transient charge trapping dynamics upon charge injection in PbS QD FETs, where source and drain electrodes were grounded all the time, we proceed to measure the transport dynamics by applying a drain bias $V_d = -5$ V (source still grounded). The same gate bias step from 0 to ±26 V was applied.

The measured transient source currents are shown in Figure 4. We found that the current transients for both holes and electrons consist of an initial sharp spike followed by a long tail, which we attribute to injection current and source-drain transport current, respectively. This is evident in the electron current (Figure 4b) as injection and transport currents have different signs due to the reverse sign between V_g and V_d. Since $V_d \ll V_g$, we expect the injection currents to follow the same

DOI: 10.1021/acs.nanolett.5b01429
Nano Lett. 2015, 15, 4657−4663

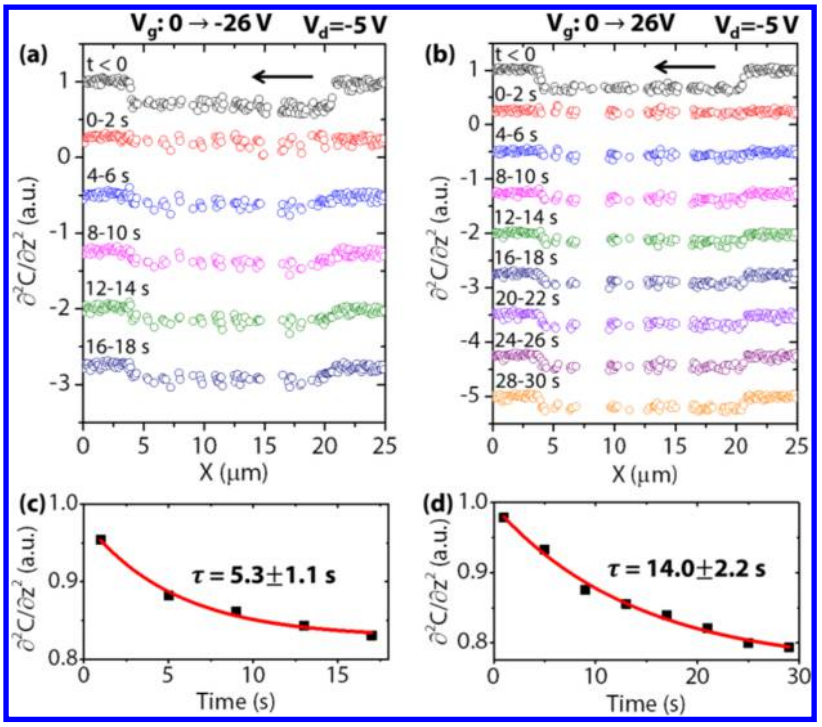

Figure 6. Capacitance ($\partial^2C/\partial z^2$) dynamics at $V_d = -5$ V, following application of a gate bias step of ∓26 V: (a,b) hole and electron dynamics, and each curve corresponds to the surface potential profile covering the source (left), channel (middle), and drain (right). The tip was scanned from right to left. (c,d) Average $\partial^2C/\partial z^2$ in the channel region as a function of time. Black dots are raw data and red lines are exponential fits.

stretched exponential decays (same time constant τ and stretching exponent β parameters) as that in Figure S2 (Supporting Information), occurring in subsecond time scales. We can thus assign the transient currents for $t > 6$ s (when injection currents are negligible) to pure transport currents, which are best fitted with exponential decays shown in the insets of Figure 4a,b. For holes and electrons, we obtained τ = 5.0 s and τ = 8.7 s for the transport current, respectively. These time constants are similar to the capacitance transients in Figure 2e,f, revealing that carrier trapping is likely the major factor responsible for the decay in transport current, which is proportional to the density of mobile carriers

$$J = en\mu E \tag{6}$$

Here J is the current density, n is the mobile carrier density, μ is the mobility, and E is the in-plane electric field. A decrease in n results in a decrease in J, provided that μ does not change significantly.

Under a finite drain bias, the local surface potential cross section along the channel reveals the electric field distribution ($E = \partial V_{sf}/\partial_x$) from which we can infer the transport mechanism (Ohmic, space-charge-limited, contact-limited, etc.). We thus analyzed the transient V_{sf} distributions upon the application of gate bias, as shown in Figure 5a,b. We can see that V_{sf} profile remains unchanged during hole injection and transport (Figure 5a), with linear decrease from source to drain characteristic of Ohmic conduction. No voltage drop is observed at the source and drain contacts, revealing that the metal−semiconductor contact is also Ohmic, as expected since the Fermi level of Au and the valence band of the PbS QDs are well aligned.[12] In contrast, the V_{sf} profile in the n-channel (electron transport) shows a transient voltage drop at the negatively biased drain electrode from which electrons were injected (Figure 5b), although Ohmic conduction inside the channel is still preserved (as evident by the linear V_{sf} decrease inside the channel). As shown in Figure 5c, the voltage drop at the drain contact follows exponential decay, decreasing from ∼2 V at t = 0 to ∼0.3 V at t = 28 s. The contact resistance is thus 2/3 of the channel resistance in the beginning and negligible in the end. However, the time constant of the contact voltage drop (ΔV) is 11.6 s, similar to that of the electron transport current (I) (Figure 4b). Therefore, the contact resistance ($\Delta V/I$) is roughly constant with a value of ∼5 GΩ, while the channel resistance increases during the nonequilibrium charge injection and transport process. The contact resistance is likely due to the ∼0.3 eV mismatch of the IGS position with that of the Au Fermi level.[12] The fact that the contact resistance remains unchanged further supports our proposed carrier trapping mechanism (Figure 3c), where the Fermi level of the injected carriers only slightly changes during the charge trapping process.

Besides the current and surface potential transients, the transient capacitance distribution was also recorded and shown in Figure 6. We can see that the capacitance is nearly the same everywhere in the channel at any given time, for both hole and electron transport, confirming that the transport of both carriers is Ohmic with uniform mobile carrier density in the channel. The average $\partial^2C/\partial z^2$ in the p-channel decays exponentially with τ = 5.3 s, nearly the same as that of the transport current, further validating the conclusion that current decay is a result of carrier trapping. In the n-channel, the average $\partial^2C/\partial z^2$ decays also exponentially with τ = 14.0 s, a little larger than that of the electron transport current. This is likely due to the large transient contact resistance that accelerates the transport current decay.

Discussion and Conclusion. The time constants of the transients are summarized in Table 1. We can see that the time scale of the transport current, surface potential, and capacitance

DOI: 10.1021/acs.nanolett.5b01429
Nano Lett. 2015, 15, 4657−4663

Table 1. Time Constants of Various Transient Parameters

physical parameter	hole response time (s)	electron response time (s)
transport current (@ $V_d = -5$ V)	5.0	8.7
surface potential (@ $V_d = 0$)	2.8	11.0
$\partial^2 C/\partial z^2$ (@ $V_d = 0$)	3.7	9.5
$\partial^2 C/\partial z^2$ (@ $V_d = -5$ V)	5.3	14.0
ΔV at injection electrode (@ $V_d = -5$ V)	N/A	11.6
contact resistance (@ $V_d = -5$ V)	N/A	constant

are of the same order for holes and for electrons, although the response time for electrons is always ∼2−3 times as large as that of holes. These results agree with previously measured current hysteresis in PbS QD thin film FETs.[13] Our results on the spatial and time-resolved surface potential and capacitance dynamics allow us to differentiate the injection and transport current, which are convoluted in the source-drain current, and directly obtain the total carrier density and mobile carrier density.

We found that the surface potential and capacitance gradually return to their original value after setting the gate bias back to zero, revealing that the trapping behavior is reversible. These reversible trapping and detrapping behavior have been observed in many disordered semiconductor systems, such as organic semiconductors, amorphous Si, and metal oxide films.[19−23] We thus propose that there can be similar mechanisms governing the hysteresis behavior in different materials. In our QD system, the correlation of surface potential and capacitance transients reveals that electrons/holes are initially injected into the conductive IGS/$1S_h$ states and subsequently are gradually trapped into lower energy states. If these trapping states are static electronic defects, they have to lie in the ∼0.2 eV gap between the IGS and $1S_h$ states. These shallow states (∼0.1 eV from band edge) will likely have a fast charge trapping rate (in the scale of fs−μs). Thus, pure electronic transitions involving static states may not account for the observed transient behavior. This leads us to propose that the trap states are created by some reversible chemical reactions induced by the injected charges. These dynamic trap states therefore are not necessarily located between the IGS and $1S_h$ states. For example, the dynamic electron traps shown in Figure 3c can be lower than the $1S_h$ state. Before charge injection, these traps do not exist; after injection, traps are dynamically created and filled.

One possible origin of these dynamic traps is reactions involving hydroxyl and hydrogen related species that are commonly observed impurities in these disordered systems.[19−23] For example, the following reactions may occur activated by the injected charges:[24]

$$O_2 + 2H_2O + 4e^- \leftrightharpoons 4OH^-$$

$$O_2 + 4H^+ + 4e^- \leftrightharpoons 2H_2O$$

These reactions will turn the charge carriers into hydroxyl and hydrogen ions that are much less mobile than electrons, which can be responsible for the observed exponential decay of mobile carrier density in the time scale of seconds. For the PbS QD systems, it has been shown before that OH^- and O_2 are usually present on the QD surface.[12,25] Therefore, the above reactions are likely to occur during charge injection. Since the $1S_h$ states are more delocalized than the IGS (induced by local defects), it is reasonable that holes in the $1S_h$ states are more easily captured by surface impurities, resulting in faster reactions compared to electrons in the IGS.

To check the validity of the proposed mechanism, we performed control measurements of current transients in an environment with higher humidity and oxygen level and found that the time constants are much smaller (Supporting Information). This supports our conclusion since higher H_2O and O_2 concentration on the QD surface is expected to induce a higher charge capture rate. Moreover, we found that these changes are reversible as long as the exposure time to higher humidity environment is short.

Additionally, we measured the drain current−drain bias curves with a closed-loop scan in inert atmosphere, while the gate bias was set to zero (Supporting Information). A hysteresis loop was observed, indicating that charge injection induces a reversible change in the film resistance. The results resemble that of cyclic voltammetry, which is a good indication of the occurrence of electrochemical charging/discharging processes. Such hysteresis behavior was also reported in scanning tunneling spectroscopy results on WS_2 nanoparticles,[26] where the hysteresis in tunneling current was also explained in terms of electrochemical processes. These results are in support of our proposed dynamic, electrochemical trapping mechanism.

Although we cannot completely rule out other possibilities responsible for the hysteresis in QD FETs, such as surface structural rearrangements[27] and ligand diffusion,[28] our first observation of the surface potential and capacitance dynamics in QD systems allows us to directly determine the decay of carrier density and identify the dynamic trapping mechanism. In terms of the effect of the gate dielectric on the hysteresis behavior, we do not expect the SiO_2 to play a role in the observed transients. It has been previously observed that charge trapping on the unpassivated SiO_2 surface occurs in the scale of hours upon the application of a gate bias,[23] which is also confirmed by our own measurements (not shown here). OTS passivation removes most of the SiO_2 surface traps,[23] so that longer hysteresis is expected. Moreover, previous measurements of the PbS QD FETs with different gate dielectric materials revealed that the transient current decay is independent of the choice of dielectric.[13] Therefore, our measured transient phenomena are due to the intrinsic properties of PbS QDs.

In conclusion, we found that charge carriers are dynamically trapped in the scale of seconds upon injection into PbS quantum dot films, which are likely associated with reversible chemical reactions possibly involving hydrogen and oxygen containing species. These traps, though detrimental to field effect transistors, may find applications in photoconductors where carrier trapping can lead to higher lifetime and photoconductive gain.[2,11] Long-lived traps can also be utilized for memory devices.[29] By controlling the surface chemistry of QDs, we can potentially manipulate these dynamics to achieve desirable device performances.

■ ASSOCIATED CONTENT

Supporting Information

Sample preparation, cross-section profile of topography and surface potential, injection current transients, FET pattern, current transients in a higher humidity environment, and drain current − drain bias closed-loop curve. The Supporting Information is available free of charge on the ACS Publications website at DOI: 10.1021/acs.nanolett.5b01429.

DOI: 10.1021/acs.nanolett.5b01429
Nano Lett. 2015, 15, 4657−4663

AUTHOR INFORMATION

Corresponding Author

*E-mail: mbsalmeron@lbl.gov.

Notes

The authors declare no competing financial interest.

ACKNOWLEDGMENTS

We thank Dr. L.-W. Wang and Dr. D. Zherebetskyy for helpful discussions. This work was supported by the "Self-Assembly of Organic/Inorganic Nanocomposite Materials" program, KC3104, Office of Science, the Office of Basic Energy Sciences (BES), Materials Sciences and Engineering (MSE) Division of the U.S. Department of Energy (DOE) under Contract No. DE-AC02-05CH11231. It used resources of the Molecular Foundry, a DOE Office of Science user facility. Q.C. was supported by a Miller fellowship from Miller Institute for Basic Research in Science at UC Berkeley.

REFERENCES

(1) Talapin, D. V.; Murray, C. B. *Science* **2005**, *310*, 86−89.
(2) Konstantatos, G.; Sargent, E. H. *Nat. Nanotechnol.* **2010**, *5*, 391−400.
(3) Chuang, C.-H. M.; Brown, P. R.; Bulović, V.; Bawendi, M. G. *Nat. Mater.* **2014**, *13*, 796−801.
(4) Kim, D. K.; Lai, Y. M.; Diroll, B. T.; Murray, C. B.; Kagan, C. R. *Nat. Commun.* **2012**, *3*, 1216.
(5) Zhitomirsky, D.; Voznyy, O.; Levina, L.; Hoogland, S.; Kemp, K. W.; Ip, A. H.; Thon, S. M.; Sargent, E. H. *Nat. Commun.* **2014**, *5*, 3803.
(6) Wolkin, M. V.; Jorne, J.; Fauchet, P. M.; Allan, G.; Delerue, C. *Phys. Rev. Lett.* **1999**, *82*, 197−200.
(7) Nagpal, P.; Klimov, V. I. *Nat. Commun.* **2011**, *2*, 486.
(8) Califano, M.; Franceschetti, A.; Zunger, A. *Nano Lett.* **2005**, *5*, 2360−2364.
(9) Cordones, A. A.; Scheele, M.; Alivisatos, A. P.; Leone, S. R. *J. Am. Chem. Soc.* **2012**, *134*, 18366−18373.
(10) Shimizu, K. T.; Neuhauser, R. G.; Leatherdale, C. A.; Empedocles, S. A.; Woo, W. K.; Bawendi, M. G. *Phys. Rev. B* **2001**, *63*, 205316−205320.
(11) Konstantatos, G.; Badioli, M.; Gaudreau, L.; Osmond, J.; Bernechea, M.; de Arquer, F. P. G.; Gatti, F.; Koppens, F. H. L. *Nat. Nanotechnol.* **2012**, *7*, 363−368.
(12) Zhang, Y.; Zherebetskyy, D.; Bronstein, N. D.; Barja, S.; Lichtenstein, L.; Schuppisser, D.; Wang, L.-W.; Alivisatos, A. P.; Salmeron, M. *Nano Lett.* **2015**, *15*, 3249−3253.
(13) Osedach, T. P.; Zhao, N.; Andrew, T. L.; Brown, P. R.; Wanger, D. D.; Strasfeld, D. B.; Chang, L.; Bawendi, M. G.; Bulović, V. *ACS Nano* **2012**, *6*, 3121−3127.
(14) Ip, A. H.; Thon, S. M.; Hoogland, S.; Voznyy, O.; Zhitomirsky, D.; Debnath, R.; Levina, L.; Rollny, L. R.; Carey, G. H.; Fischer, A.; Kemp, K. W.; Kramer, I. J.; Ning, Z. J.; Labelle, A. J.; Chou, K. W.; Amassian, A.; Sargent, E. H. *Nat. Nanotechnol.* **2012**, *7*, 577−582.
(15) Luther, J. M.; Law, M.; Song, Q.; Perkins, C. L.; Beard, M. C.; Nozik, A. J. *ACS Nano* **2008**, *2*, 271−280.
(16) Liu, Y.; Gibbs, M.; Puthussery, J.; Gaik, S.; Ihly, R.; Hillhouse, H. W.; Law, M. *Nano Lett.* **2010**, *10*, 1960−1969.
(17) Zhang, Y.; Ziegler, D.; Salmeron, M. *ACS Nano* **2013**, *7*, 8258−8265.
(18) Silveira, W. R.; Marohn, J. A. *Phys. Rev. Lett.* **2004**, *93*, 116104.
(19) Lang, D. V.; Chi, X.; Siegrist, T.; Sergent, A. M.; Ramirez, A. P. *Phys. Rev. Lett.* **2004**, *93*, 076601.
(20) Gupta, D.; Yoo, S.; Lee, C.; Hong, Y. *IEEE Trans. Electron Devices* **2011**, *58*, 1995−2002.
(21) Deane, S. C.; Wehrspohn, R. B.; Powell, M. J. *Phys. Rev. B* **1998**, *58*, 12625−12628.
(22) Nicolai, H. T.; Kuik, M.; Wetzelaer, G. A. H.; de Boer, B.; Campbell, C.; Risko, C.; Brédas, J. L.; Blom, P. W. M. *Nat. Mater.* **2012**, *11*, 882−887.
(23) Chua, L. L.; Zaumseil, J.; Chang, J. F.; Ou, E. C. W.; Ho, P. K. H.; Sirringhaus, H.; Friend, R. H. *Nature* **2005**, *434*, 194−199.
(24) Chakrapani, V.; Angus, J. C.; Anderson, A. B.; Wolter, S. D.; Stoner, B. R.; Sumanasekera, G. U. *Science* **2007**, *318*, 1424−1430.
(25) Zherebetskyy, D.; Scheele, M.; Zhang, Y.; Bronstein, N.; Thompson, C.; Britt, D.; Salmeron, M.; Alivisatos, P.; Wang, L.-W. *Science* **2014**, *344*, 1380−1384.
(26) Azulay, D.; Kopnov, F.; Tenne, R.; Balberg, I.; Millo, O. *Nano Lett.* **2006**, *6*, 760−764.
(27) Voznyy, O.; Thon, S. M.; Ip, A. H.; Sargent, E. H. *J. Phys. Chem. Lett.* **2013**, *4*, 987−992.
(28) Voznyy, O. *J. Phys. Chem. C* **2011**, *115*, 15927−15932.
(29) Busche, C.; Vilà-Nadal, L.; Yan, J.; Miras, H. N.; Long, D.-L.; Georgiev, V. P.; Asenov, A.; Pedersen, R. H.; Gadegaard, N.; Mirza, M. M.; Paul, D. J.; Poblet, J. M.; Cronin, L. *Nature* **2014**, *515*, 545−549.

DOI: 10.1021/acs.nanolett.5b01429
Nano Lett. 2015, 15, 4657−4663